



	<b>Experiment title:</b> Phase diagram and metastable phase formation studies of Nb bearing gamma TiAl turbine blade alloys	<b>Experiment number:</b> MA-179
<b>Beamline:</b> ID15 A	<b>Date of experiment:</b> from: 24.01.2007 to: 30.01.2007	<b>Date of report:</b> 31.08.2007
<b>Shifts:</b> 15	<b>Local contact(s):</b> Dr. Thomas Buslaps	<i>Received at ESRF:</i>
<b>Names and affiliations of applicants</b> (* indicates experimentalists): <b>Dirk Holland-Moritz<sup>1,*</sup>, Wolfgang Löser<sup>2</sup>, Olga Shuleshova<sup>2,*</sup>, Helena Hartmann<sup>1,*</sup>, Thomas Volkmann<sup>1,*</sup>, Norbert Mattern<sup>2,*</sup>, and Hans-Günther Lindenkreuz<sup>2,*</sup></b>  <sup>1</sup> Institut für Materialphysik im Weltraum, DLR, D-51170 Köln, Germany <sup>2</sup> IFW Dresden, Institut für Festkörperforschung, Postfach 270116, D-01171 Dresden, Germany		

## Report:

Over the last decades  $\gamma$  titanium-aluminide based alloys are a subject of an impressive amount of research forced by their superior properties at elevated temperatures. However, despite the great commercial interest for automotive and aerospace applications there still remains a necessity to improve the material properties by modifying processing and alloy composition. In particular, Niobium bearing alloys can provide higher yield stress, improved room temperature ductility, and enhanced oxidation resistance. An Integrated Project IMPRESS, an acronym for Intermetallic Materials Processing in Relation to Earth and Space Solidification, which joins more than 40 European partners, was started in November 2004 [1]. One of the aims of this project is to optimise the casting processes and post-solidification heat-treatment of  $\gamma$  titanium-aluminide based alloys, in order to deliver high-quality turbine blades.

Despite, the many studies there are still serious discrepancies in the ternary Ti-Al-Nb phase diagram. In the composition range  $\text{Ti}_{41-51}\text{Al}_{44-49}\text{Nb}_{5-10}$  prospective for commercial  $\gamma$  titanium aluminides, reliable experimental data for temperatures  $> 1400^\circ\text{C}$  are missing and even liquidus projections published by different authors [2-5] are seriously at variance concerning the solidification range of the cubic  $\beta$ -Ti (A2), the hexagonal  $\alpha$ -Ti (A3) and the intermetallic  $\gamma$ -TiAl ( $L1_0$ ) phase, which may be formed during solidification in this compositional regime. For different alloy compositions the phases that are in equilibrium with the liquid at the liquidus temperature according to the various assessments [2-5] of the phase diagram are listed in table 1. The rather unexpected divergence of the various phase diagram assessments arise from two inherent complications of the Ti-Al alloys: (1) high reactivity of the melts at temperatures around  $1500^\circ\text{C}$  with alumina and even yttria crucibles (e.g. in differential thermoanalysis devices) lead to an uptake of impurities, which affect the phase equilibria, (2) the primary solidified phases undergo various solid state phase transformations on cooling and can completely disappear in the as-solidified microstructure.

Both difficulties are elegantly circumvented by combining containerless processing technique with *in-situ* diffraction techniques for determination of the phases formed during solidification. Therefore, we have

performed energy dispersive X-ray diffraction experiments on melts of different Ti-Al-Nb and Ti-Al-Nb-C-B alloys at beamline ID15A of the ESRF. The melts were containerlessly processed within an electromagnetic levitation facility specially designed for this type of experiments. The experimental setup is described elsewhere [6]. Apart from studies of the equilibrium phase diagram we have also investigated the phase selection behaviour of the alloys during non-equilibrium solidification from the metastable state of an undercooled liquid.

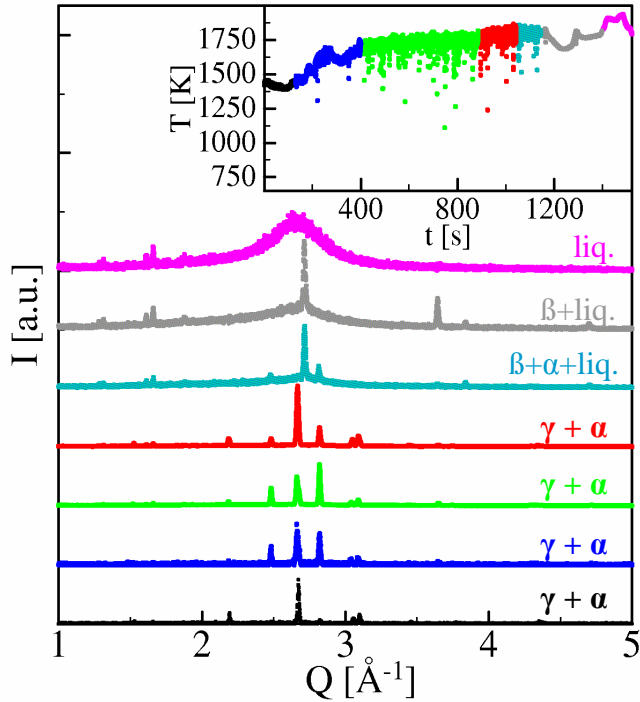


**Figure 1:** Energy dispersive X-ray diffractograms acquired during slow heating of a  $\text{Ti}_{40}\text{Al}_{50}\text{Nb}_{10}$  sample. The temperature-time profile of this experiment is shown in the insert. The different colours mark the time intervals during which the diffractograms plotted in the same colour were recorded.

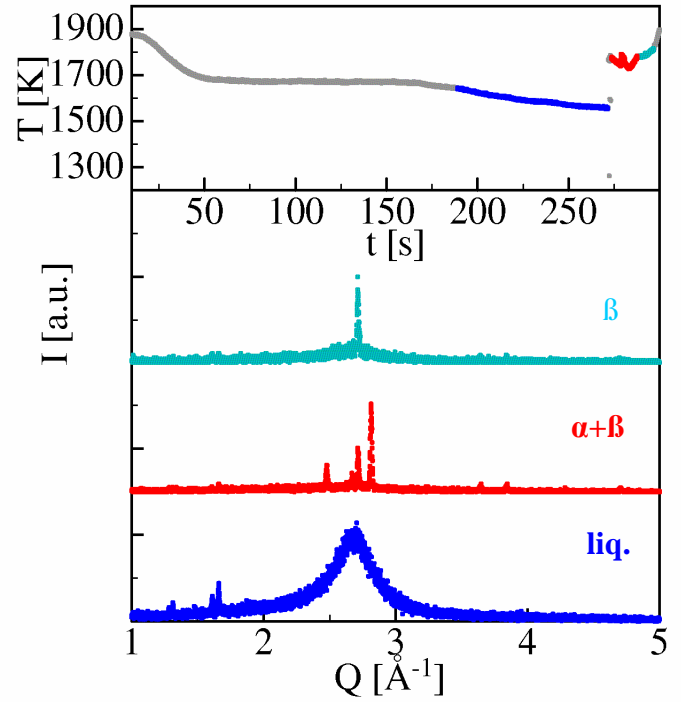


**Figure 2:** Energy dispersive X-ray diffractograms acquired during an undercooling experiment on a  $\text{Ti}_{40}\text{Al}_{50}\text{Nb}_{10}$  melt. The temperature-time profile is shown in the upper part of the figure. The different colours mark the time intervals during which the diffractograms plotted in the same colour were recorded.

As an example, figure 1 shows results of an *in-situ* diffraction experiment on a  $\text{Ti}_{40}\text{Al}_{50}\text{Nb}_{10}$  sample during slow heating. The aim of this experiment is to study the equilibrium phase diagram of Ti-Al-Nb at high temperatures. In the insert of figure 1 the temperature-time profile measured by pyrometry is shown. The different colours in the temperature-time profile mark the time intervals during which the corresponding diffractograms plotted in the same colour were recorded. At approximately 1400 K the sample consists of  $\alpha + \gamma$ . At a temperature of approximately 1800 K the phase transformation  $\alpha + \gamma$  (red spectrum)  $\rightarrow$   $\alpha + \beta + \text{liquid}$  (cyan spectrum) is observed. At a slightly higher temperature, the  $\alpha$ -phase transforms such that the sample consists of  $\beta$ -phase and liquid (grey spectrum). The small drop of the temperature signal is a result of the change of emissivity during the phase transformation and does not indicate a real decrease of the sample temperature. If the temperature is further increased, the  $\beta$ -phase melts and the sample is completely liquid (pink spectrum). Hence, our *in-situ* diffraction experiments provide direct experimental evidence that for  $\text{Ti}_{40}\text{Al}_{50}\text{Nb}_{10}$  the  $\beta$ -phase is in equilibrium with the liquid phase at the liquidus temperature. This result together with the results on the primary phase formation for the other alloys obtained under conditions close to equilibrium solidification are summarized in the last column of table 1. When comparing our results with the literature data, it becomes obvious that the *in-situ* diffraction experiments confirm the assessment of

Yamamoto [5]. Also our *in-situ* X-ray diffraction results of the phase transformations at lower temperatures (not shown in table 1) are in excellent agreement with the assessment of Yamamoto [5]

Figure 2 shows an example for an experiment on the non-equilibrium solidification of a deeply undercooled Ti<sub>40</sub>Al<sub>50</sub>Nb<sub>10</sub> melt. Starting from a temperature above the liquidus temperature of 1820 K the temperature of the sample was decreased and the melt was undercooled (compare the temperature-time profile in the upper part of figure 2). At a temperature of approximately 1580 K, corresponding to an undercooling of  $\Delta T = 240\text{K}$ , solidification sets in, indicated by a steep temperature increase due to the release of heat of fusion. While the sample is liquid before this temperature increase as proven by the diffractogram with the broad diffuse intensity maximum typical of a liquid (dark blue spectrum), after the temperature rise the diffractogram shows bragg peaks of the  $\alpha$  and the  $\beta$  phase (red spectrum). Both phases simultaneously appear during non-equilibrium solidification from the undercooled melt. If the as-solidified sample is heated, first the  $\alpha$  phase transforms, such that the sample consists only of  $\beta$  phase and liquid at temperatures closely below the liquidus temperature (light blue spectrum).

Summarizing, the unambiguous determination of phases by *in-situ* X-ray diffraction at ESRF during solidification processes provided a clear validation of the existing Ti-Al-Nb phase diagrams, which has not been possible by conventional methods.

Composition (at.%)	C. Servant [2]	N. Saunders [3]	V. Raghavan [4]	Y. Yamamoto [5]	<b>This work</b>
Ti <sub>50</sub> Al <sub>45</sub> Nb <sub>5</sub>	$\alpha$	$\beta$	$\beta$	$\beta$	<b><math>\beta</math></b>
Ti <sub>46</sub> Al <sub>46</sub> Nb <sub>8</sub>	$\alpha$	$\beta$	$\beta$	$\beta$	<b><math>\beta</math></b>
Ti <sub>45</sub> Al <sub>45</sub> Nb <sub>10</sub>	$\alpha$	$\beta$	$\beta$	$\beta$	<b><math>\beta</math></b>
Ti <sub>45</sub> Al <sub>50</sub> Nb <sub>5</sub>	$\alpha$	$\beta$	$\alpha$	$\beta$	<b><math>\beta</math></b>
Ti <sub>40</sub> Al <sub>50</sub> Nb <sub>10</sub>	$\gamma$	$\beta$	$\alpha$	$\beta$	<b><math>\beta</math></b>
Ti <sub>43</sub> Al <sub>52</sub> Nb <sub>5</sub>	$\alpha$	$\beta$	$\alpha$	$\alpha$	<b><math>\alpha</math></b>
Ti <sub>41</sub> Al <sub>54</sub> Nb <sub>5</sub>	$\gamma$	$\alpha$	$\alpha$	$\alpha$	<b><math>\alpha</math></b>
Ti <sub>35</sub> Al <sub>60</sub> Nb <sub>5</sub>	$\gamma$	$\gamma$	$\gamma$	$\gamma$	<b><math>\gamma</math></b>

**Table 1:** Phases in equilibrium with the melt at the liquidus temperature according the different assessments of the phase diagram [2-5] and as found in this work by *in-situ* X-ray diffraction.

## References

- [1] D.J. Jarvis, D. Voss, Mater. Sci. & Eng. A **413-414** (2005) 583–591.
- [2] C. Servant and I. Ansara, Ber. Bunsenges. Phys.Chem. **102**, 1189-1205 (1998).
- [3] N. Saunders, in: W. Kim, D.M. Dimiduk, and M.H. Loretto (eds.) *Gamma Titanium Aluminides 1999*, (The Minerals, Metals and Materials Society, Warrendale, PA), 183-188.
- [4] V. Raghavan, J. Phase Equilibria and Diffusion **26**, 360-368 (2005).
- [5] Y. Yamamoto and M. Takeyama. Intermetallics **13**, 965-970 (2005).
- [6] C. Notthoff, H. Franz, M. Hanfland, D.M. Herlach, D. Holland-Moritz, G. Jacobs, R. Lippok, W. Petry, and D. Platzek, J. Non-Cryst. Sol. **250-252**, 632 (1999).